RSC Advances

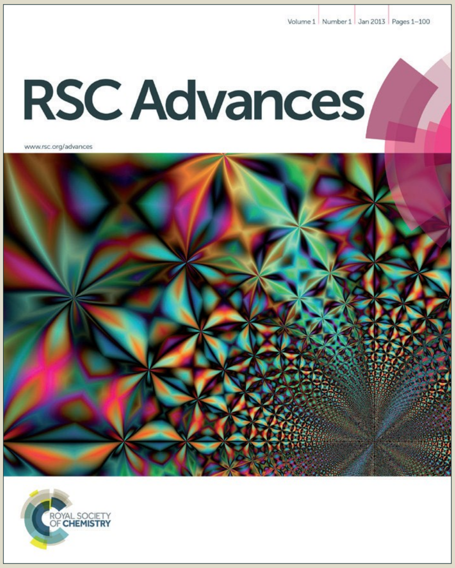

ROYAL SOCIETY OF CHEMISTRY

www.rsc.org/advances

Journal Name

ARTICLE

Received 00th January 20xx,
Accepted 00th January 20xx

DOI: 10.1039/x0xx00000x

www.rsc.org/

Accelerating the decomposition of $KMnO_4$ by photolysis and auto-catalysis: A green approach to synthesize layered birnessite-type MnO_2 assembled hierarchical nanostructure

Xiaonan Hu,[a] Liyi Shi,[b] Dengsong Zhang,*[a] Xin Zhao [a] and Lei Huang*[a]

In this work, we developed a facile, green and low-cost strategy for controllable synthesis of Birnessite-type MnO_2 (Bir-MnO_2) nanosheets assembled “desert rose”-like 3D hierarchical nanostructure and proposed a two-step growth route, namely the photolysis and followed auto-catalytic decomposition of $KMnO_4$. Bir-MnO_2 nanosheets were first obtained under the irradiation of light sources and acted as seeds for further decomposition of the excess MnO_4^- in the dark. The sizes of the Bir-MnO_2 3D hierarchical nanostructures could be readily controlled by varying the concentration of $KMnO_4$, the light sources and the pH values. Furthermore, Bir-MnO_2 nanosheets on CNTs were successfully fabricated utilizing the same strategy without the addition of any surfactants or organic templates. It is anticipated that the fabrication of Bir-MnO_2 based nanostructures and composites could be beneficial from this universal method.

Introduction

The design and fabrication of three-dimensional (3D) hierarchical nanostructures have been attracting close attention owing to their unique properties such as in the transfer of carriers inside the hierarchical nanoarchitectures and the diffusion of reactants in the interspace.[1-3] Those properties are known to be significantly affected by the tunnel size and shape of nanostructures.[4, 5] However, the tailored synthesis of complex architectures with special size and shape usually achieved at high temperature or by using organic solvents and templates, which obviously increase the production costs and technical complexity.[6] Consequently, it is highly desirable to focus on the development of environmental benign and low-cost synthetic methods that produce complex architectures to alleviate these problems.

As an important layered manganese oxide compounds, birnessite-type MnO_2 (Bir-MnO_2) consists of coplanar layers of infinite two-dimensional sheets of edge-shared MnO_6 octahedra. Their formula are normally expressed as $A_xMnO_2 \cdot yH_2O$, where A is proton H^+ or an alkali-metal cation such as K^+, Na^+ and Li^+.[7, 8] The cations and water molecules occupied in the interlayer space are exchangeable, which endows high mobility and little structural rearrangement. The distinctive layered structure provides abundant active sites for ion-exchange and molecular adsorption, which makes them very attractive in the applications of supercapacitor,[9, 10] catalysis,[11-13] ion-exchangers,[14] Li-battery,[15] and so on.[16, 17] Bir-MnO_2 with different morphologies[18-21] or loaded over different supporting matrix, for example, carbon nanotubes (CNTs) ,[22-24] graphene[25, 26] and so forth,[27, 28] have been proved to be effective in adjusting their chemical and physical properties for various applications. However, the rational design and green synthesis of 3D hierarchical Bir-MnO_2 and their composites with controllable size and morphology still remain as a significant challenge.

In this work, layered Bir-MnO_2 nanosheets assembled 3D hierarchical nanostructures were controllably synthesized through the direct decomposition of $KMnO_4$ with two steps at room temperature as illustrated in Scheme 1a. In the first step, Bir-MnO_2 nanosheets were obtained with the irradiation of lab light source, even sunlight. To the best of our knowledge, this is the first time to synthesize Bir-MnO_2 based on the well-known phenomenon that $KMnO_4$ undergoes decomposition when exposed to light. In the second step, residual $KMnO_4$ in the reacted solution was further decomposed in dark with the assistance of formed Bir-MnO_2 nanosheets by a so-called auto-catalytic effect, which leads to the formation of nanosheets assembled “desert rose”-like 3D hierarchical nanostructures. Apparently, this novel approach is straightforward and environmentally sustainability. More importantly, the above two steps could be utilized to conveniently prepare Bir-MnO_2 based composites. Herein, we also successfully loaded Bir-MnO_2 nanosheets over CNTs (Bir-MnO_2/CNTs), forming hierarchical nanostructure as illustrated in Scheme 1b.

---

a Research Center of Nano Science and Technology, Shanghai University, Shanghai 200444, P. R. China.
b Department of Chemistry, Shanghai University, Shanghai 200444, P. R. China.
*To whom correspondence should be addressed: Fax: +86-21-66136079;
Tel: +86-21-66136079;
E-mail: leihuang@shu.edu.cn (L. Huang), dszhang@shu.edu.cn (D. Zhang)

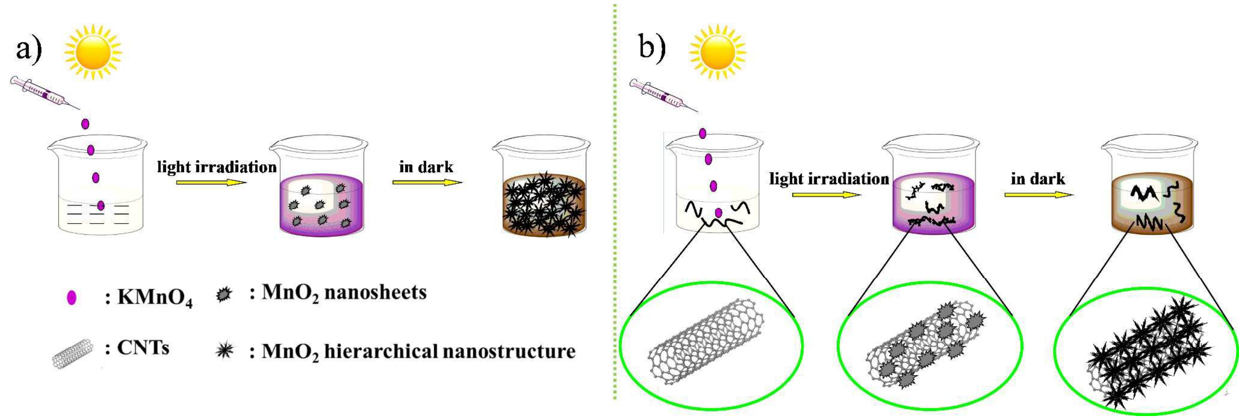

Scheme 1. Schematic illustration of the fabrication of layered Bir-MnO$_2$ assembled hierarchical nanostructure (a) and Bir-MnO2/CNTs hybrids (b).

Experimental

Preparation of layered Bir-MnO$_2$ assembled hierarchical nanostructure

The multiwalled CNTs with the diameter of 40–60 nm were purchased from Shenzhen Nanotech Nano Pon Co. Ltd (China). All the other chemical reagents are of analytical grade from Sinopharm Chemical Reagent Company and used as received without further purification.

Two steps were involved in the preparation of layered Bir-MnO$_2$ assembled hierarchical nanostructure. The first step is the photolysis of KMnO$_4$. In a typical preparation process, 0.079g of KMnO$_4$ powders was completely dissolved in 20mL of deionized water under magnetic stirring for about 10 min to form a dark purple solution. The as-obtained KMnO$_4$ solution subsequently was injected with a speed of 40mL/h controlled by a syringe into the Pyrex reaction cell containing 30mL of deionized water in the irradiation of UV light (mercury lamp with the wavelength of 254 nm). The injection process was terminated in 30 min but the solution was still irradiated by UV light for 1.5-7.5h. In other words, the total irradiation duration was 2.0-8.0h. In the second step, the obtained suspension then was transferred in a beaker and placed in dark for a few more days. Finally, the products were collected via filtering and rinsing thoroughly with distilled water for several times to remove residual KMnO$_4$. The sample was then freeze-dried overnight for further use.

The photodecomposition reactions were carried out in a Pyrex reaction cell equipped with a circulating cooling water system to keep the whole irradiation process at 10^{o}C. The whole Pyrex reaction cell and the light source, a 32W mercury lamp, were placed in a darkroom to avoid the influence of indoor light. In other comparative experiments, fluorescent lamp was used as the visible light source. The pH value of the KMnO$_4$ solution was adjusted by H$_2$SO$_4$.

Fabrication of Bir-MnO$_2$ /CNTs hybrid nanostructure

Briefly, the CNTs were first refluxed in a 65% nitric acid at 140^{o}C for 6h. Afterwards, 10mg purified CNTs was dispersed in 30 mL of deionized water under an ultrasonic bath. The followed photodecomposition procedure was exactly similar with the preparation process of layered Bir-MnO$_2$. The whole irradiation process and statically aging procedure at room temperature were lasted for 2h and 5 days, separately. The obtained products were harvested by filtration and washing fully with distilled water before freeze-drying overnight.

Characterizations

The X-ray diffraction pattern (XRD) measurements were performed on a Rigaku D/MAX2200V PC X-ray diffractometer employing a Cu Kα (40kv, 40mA) radiation and a secondary beam graphite monochromator from 10^{o} to 90^{o} at a step size of 0.020 (2θ). The morphologies and microstructures were characterized by Transmission electron microscopic (TEM, JEM-200CX) and High resolution TEM (HRTEM, JEM-2100F), respectively. Energy-dispersive X-ray (EDX) analysis and elemental mapping were recorded to obtain the component of the samples by an Inca Energy 200 TEM system from Oxford instruments. The Ultraviolet-Visible absorption spectra were recorded on a double beam UV-vis spectrophotometer (760CRT). N$_2$ adsorption–desorption isotherms were obtained at 77 K on Autosorb iQ2-2MP-C (Quantachrome). The specific surface areas were determined using the Brunauer–Emmett–Teller (BET) equation. The pore volumes and average pore diameters were determined by the Barrett-Joyner-Halenda (BJH) method from the desorption branches of the isotherms.

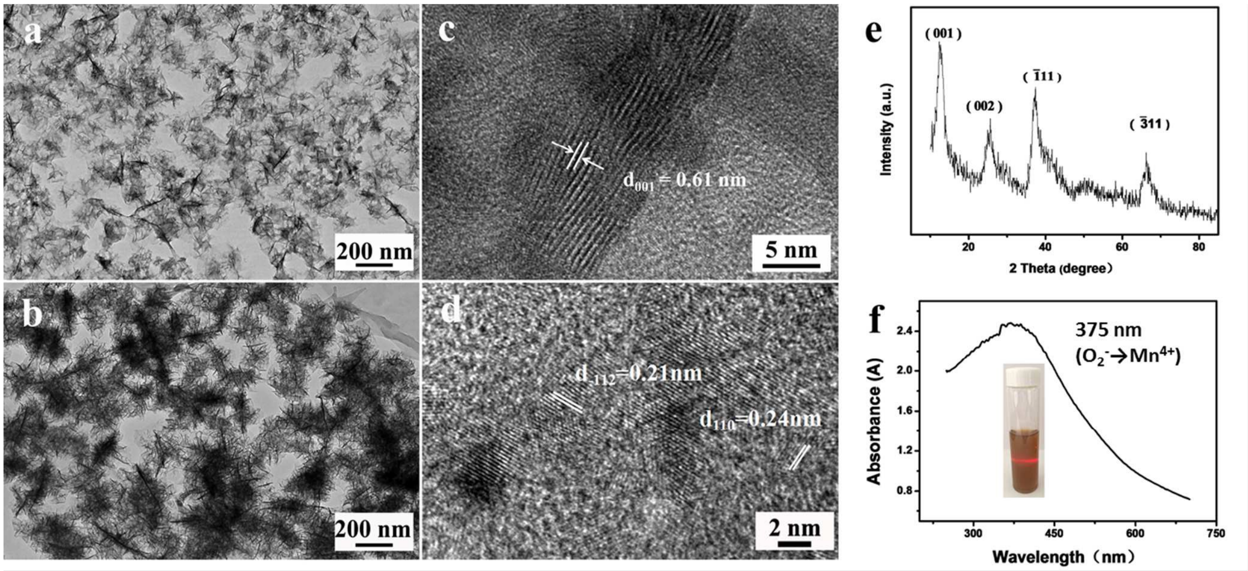

Fig. 1 TEM images of Bir-MnO_2 nanostructures obtained with different reaction durations: (a) 2h of irradiation under UV light and (b) aging for further 5 days (Bir-MnO_2 assembled hierarchical nanostructure). (c-d) HRTEM images of Bir-MnO_2 assembled hierarchical nanostructure (e) XRD pattern of Bir-MnO_2 assembled hierarchical nanostructure (f) UV-vis absorption spectra and photograph (inset) of Bir-MnO_2 assembled hierarchical nanostructure at concentration of 320 mg L^{-1}.

Results and discussion

It is well-known that the decomposition of MnO_4^- in neutral solutions is a spontaneous reaction which can be described by the following reaction equations.[29]

$$4MnO_4^- + 2H_2O \rightarrow 4MnO_2 + 4OH^- + 3O_2 \quad (1)$$

Nevertheless, this reaction was considered to be extremely slow.[30] Our experiments also proved this statement. No MnO_2 precipitate was observed when the $KMnO_4$ solution was aged in dark for more than 10 days. Nonetheless, the situation would change when light was applied to irradiate the $KMnO_4$ solution at room temperature. Black MnO_2 precipitates were obtained after two hours of irradiation. TEM images (Fig. 1a) showed that the MnO_2 nanostructures were composed of many curly and interlaced nanosheets with an average diameter of around 50 nm (Fig. 1a). Very interestingly, the nanosheets continued to grow up without the irradiation when the suspension was further aged in dark for a period of time. Fig. 1b depicted that the morphology became more complicated and formed to be "desert rose"-like 3D hierarchical nanostructures after 5 days of aging. The sizes of the nanostructures noticeably increased to about 200 nm. HRTEM measurement has been carried out to provide insights into the detailed morphologies and crystalline structures of the as-obtained Bir-MnO_2 at the atomic level. The lateral view in Fig. 1c confirmed the layered structure of the MnO_2 nanosheets with an interlayer spacing of 0.61 nm. Herein, the interlayer spacing is smaller than the interplanar space of representative birnessite (normally 0.7 nm) which is presumably due to the occurrence of dehydration under the electron beam bombardment.[31, 32] The bending of the nanosheets indicate that the structure is flexible in nature. Fig. 1d reveals that the nanosheets are an assembly of many crystalline particles with sizes of about 5-10 nm. The clear lattice spacing of 0.21 and 0.24 nm correspond to the (-112) and (110) planes, respectively. It seems that the as-prepared Bir-MnO_2 crystal under irradiation have an anisotropic crystalline structure. The continuous growth of the polycrystalline is prone to form interconnected MnO_2 nanosheets orientated in many different directions, forming the "desert rose"-like 3D hierarchical nanostructures.

The XRD pattern (Fig. 1e) evidenced that the characteristic peaks are readily indexable to K-birnessite-type layered MnO_2 (JCPDS card no.80-1098, monoclinic, a = 5.15 Å, b = 2.84 Å, c = 7.17 Å), in which the diffraction peaks at 2θ of 12.5°, 25.2°, 37.3°, 63.3° correspond to the (001), (002), (-111), (-311) plane, respectively. The composition of Bir-MnO_2 was further evaluated by EDX spectroscopy, which verifies the atomic ratios of K/Mn/O being 0.15:1:3.2, suggesting a small amount

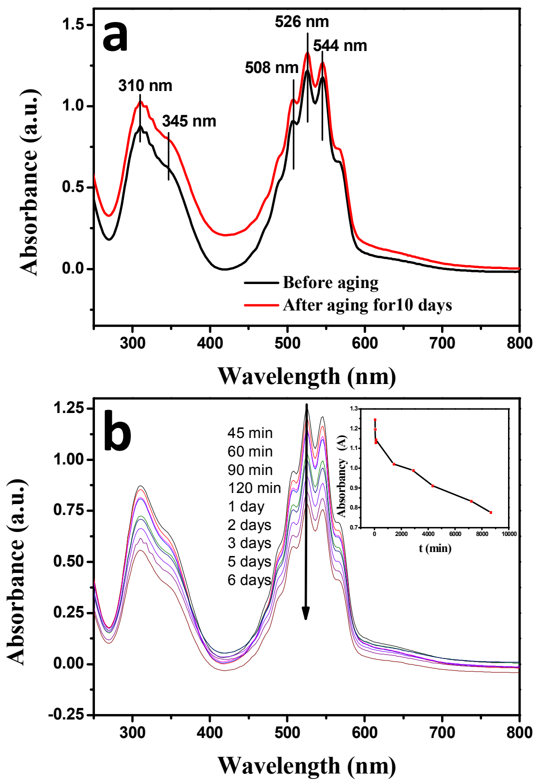

Fig. 2 (a) UV-vis absorption spectra of $KMnO_4$ solutions before and after aging for 10 days in the dark. (b) the evolution of UV-vis absorption spectra of $KMnO_4$ solution at different reaction duration and the absorbance at 524 nm plotted against the treatment time (inset).

of K^+ ions in the interlayer to balance the net negative charge of the MnO_2 layer (Table S1).[33]

Benefited from the open and porous 3D structure, the as-prepared Bir-MnO_2 delivers a high BET specific surface area of 85.1 m^2g^{-1} and a total pore volume of 2.018 cm^3/g with mesoporous texture by N_2 adsorption-desorption measurement at 77K (Fig. S1 and Table S2). Additionally, the Bir-MnO_2 was proved to be highly soluble in aqueous solution and exhibited Tyndall light scattering (the inset of Fig. 1f). Corresponding UV-vis adsorption spectrum (Fig. 1f) displays a broad absorption peak over a wavelength range of 250-700nm centered at around 375nm, which is a typical optical characteristic of the layered MnO_2 nanosheets in conformity with previous investigation[34-37] and corresponds to $Mn^{4+} \leftarrow O_2^-$ charge transfer transitions.[38]

To understand the formation route of Bir-MnO_2 nanosheets assembled hierarchical nanostructures, the decomposition process of $KMnO_4$ was detected by the evolution of UV-vis absorption spectra as shown in Fig. 2. The absorption peaks at 508, 526 and 544 nm assigned to the orbitally allowed transition $^1A_1 \rightarrow {}^1T_2$ ($t_1 \rightarrow 2e$), while the bands at about 310 and 345nm are associated with a $^1A_1 \rightarrow {}^1T_2$ ($3t_2 \rightarrow 2e$) transition.[39] Firstly, it was worth noting that the concentration of $KMnO_4$ almost didn't change without the irradiation of light after 10 days of aging in dark, indicating that the direct decomposition of $KMnO_4$ is hard to happen due to the kinetically unfavorable reaction as mentioned above. Strikingly, the concentration of $KMnO_4$ continued to decrease in the irradiation of UV-vis light and the followed aging step in dark. Based on this observation, a conclusion could be drawn that light can accelerate the decomposition of the $KMnO_4$. Meanwhile, the formed Bir-MnO_2 nanosheets were significant to the successive decomposition of $KMnO_4$ in dark. It is also noticed that two hours of irradiation caused the decrease of concentration almost equal to that aged for one day, indicating that light is much more beneficial to the decomposition of $KMnO_4$ than the followed aging process in the dark. The importance of irradiation was further confirmed by the evolution of morphologies with the increase of irradiation duration. The sizes of the Bir-MnO_2 nanosheets increased to 80 nm and 100 nm with prolonging the irradiation duration up to 4 h (Fig. S2a) and 8 h (Fig. S2b). Above results demonstrated that the irradiation is beneficial to the decomposition of $KMnO_4$ and the concomitant formation of Bir-MnO_2 nanostructure.

Based on the above observations, the formation of 3D "desert rose"-like nanostructured Bir-MnO_2 could be generalized into two steps as illustrated in Scheme 1a. The first step was carried out in the irradiation of UV/Vis light. Nuclear and growth of Bir-MnO_2 were involved in this stage, forming curly and interlaced nanosheets. In the second step, the formed Bir-MnO_2 nanosheets act as seeds for further decomposition of the excess MnO_4^- in the dark. The continued self-assembled and anisotropic growth of layered MnO_2 brought the formation of nanosheets assembled "desert rose"-like 3D hierarchical nanostructures. Obviously, the driving force involved in the two steps was different and could be addressed as following. It is well known that the decomposition of MnO_4^- in neutral solutions is thermodynamically favorable but dynamically impracticable. However, the rate of the decomposition of $KMnO_4$ could be accelerated by the decrease of activation energy. In the first step, it is understandable that the absorption of photons would make MnO_4^- excite from the ground state to the excited

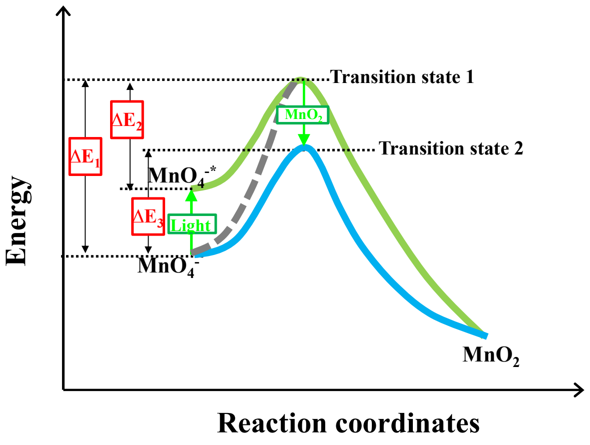

Fig. 3 Schematic illustration of the change of activation energy during the reaction of $KMnO_4$ decomposition

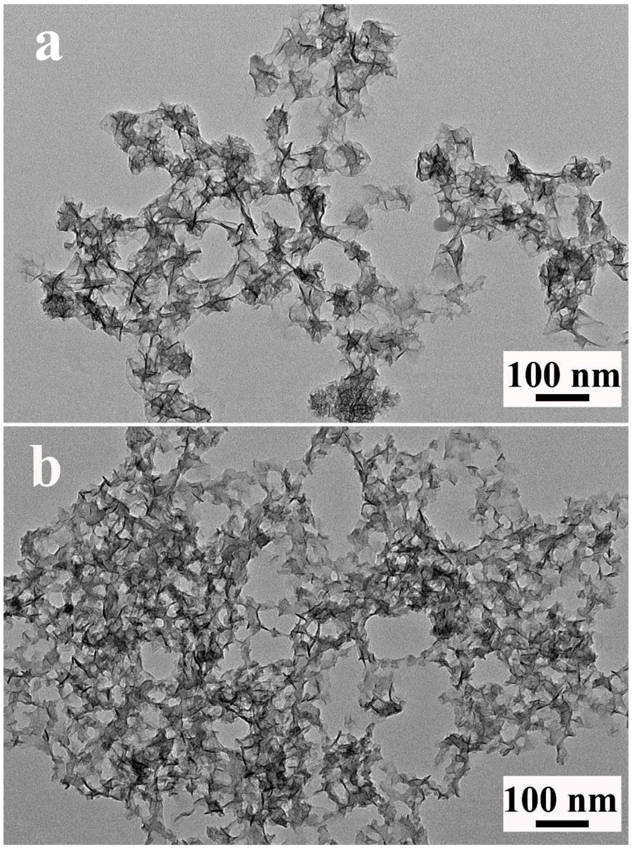

Fig.4 TEM images of Bir-MnO_2 samples obtained at different $KMnO_4$ concentrations: (a) 0.01M and (b) 0.005M. Here, the $KMnO_4$ with special concentrations were directly irradiated under UV light instead of injection.

state, which is much easier to decompose. In other words, the activation energy for the decomposition of MnO_4^- decreases. As elucidated in Fig. 3, without irradiation, the activation energy for the decomposition of MnO_4^- is ΔE_1. In the irradiation, the initial energy state increased, thus the activation energy decreased to ΔE_2. In the aging process under dark ambient, MnO_4^- was at the ground state. However, it has been well demonstrated that MnO_2 was a good catalyst to decompose the $KMnO_4$, namely the auto-catalytic effect,[40] which means that the activation energy could also decreased from ΔE_1 to ΔE_3 by the new formed Bir-MnO_2.

Based on the above understanding, it is feasible to obtain the key factors which affect the synthesis process then to controllably prepare the Bir-MnO_2 nanostructures. According to equation 1, the factors that could change the reaction rate are the concentration of $KMnO_4$, the partial pressure of O_2 and the light sources. In fact, pH value is another important factor that affects the reaction kinetics when the decomposition of MnO_4^- is in acid solutions as demonstrated in equation 2.[31] Besides, temperature is of course a crucial factor, but it is out of the discussion in this work since the temperatures were kept at room temperature in all experiments. It is anticipated that the change of decomposition rate would have influences on the morphologies. For example, higher decomposition rate would boost the nuclear and growth process， inducing larger sizes of 3D hierarchical nanostructures.

$$4MnO_4^- + 4H^+ \rightarrow 4MnO_2 + 3O_2 + 2H_2O \qquad (2)$$

The influence of concentrations of $KMnO_4$ solution was first studied. The $KMnO_4$ solutions with the concentrations of 0.010, 0.005 and 0.001 M were directly irradiated by the UV-visible light. It was found out that almost no MnO_2 samples were obtained at the concentrations of 0.001 M, which could probably be ascribed to the low decomposition rate or the limited Bir-MnO_2 which was difficult to be collected. The morphologies of the obtained Bir-MnO_2 at the concentrations of 0.01 and 0.005 M were shown in Fig. 4. The “desert rose”-like Bir-MnO_2 were also obtained. Obviously, the size of the nanostructure decreased from 60 to 30nm with the decrease of the concentration of $KMnO_4$ solution from 0.010 to 0.005 M, indicating that the decrease of decomposition rate decreases the particle size.

The influence of the pH values of the initial reaction system on the morphologies of the Bir-MnO_2 was further investigated. H_2SO_4 was used to adjust the pH of $KMnO_4$ solutions before injecting into the 30mL aqueous solution. The TEM and SEM images in Fig. 5 clearly showed that nanosheets assembled 3D hierarchical nanostructures with uniform sizes were obtained at lower pH values. The average diameters of the nanostructures increased from around 200 to 500 nm and 2 μm when the pH value decreased from 5.0 to 3.0 and 1.0, respectively. Conspicuously, the change of particle size was much larger compared with that brought by the concentration of $KMnO_4$ solution, which is probably due to that the change of the pH value leads to prominent variation in the concentration of H^+ than the concentration of the $KMnO_4^-$. For

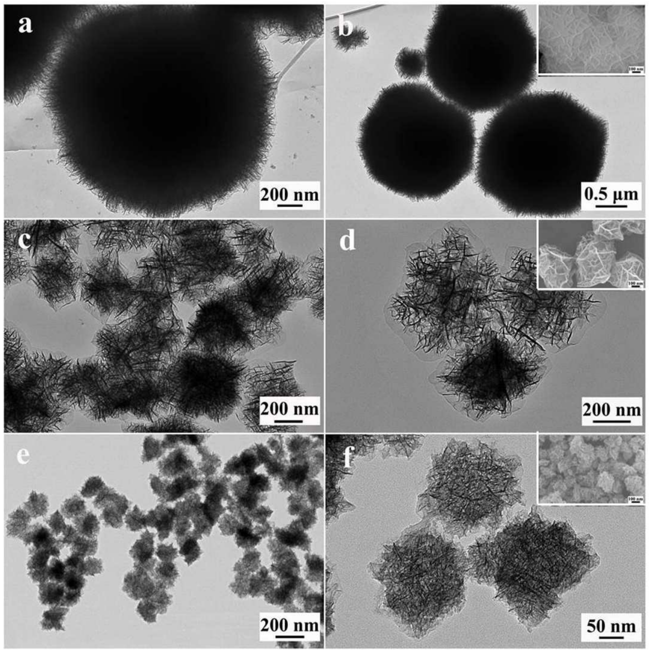

Fig. 5 TEM and SEM images (inset) of Bir-MnO_2 assembled hierarchical nanostructure obtained at different pH values: (a,b) pH=1, (c,d) pH=3, (e,f) pH=5.

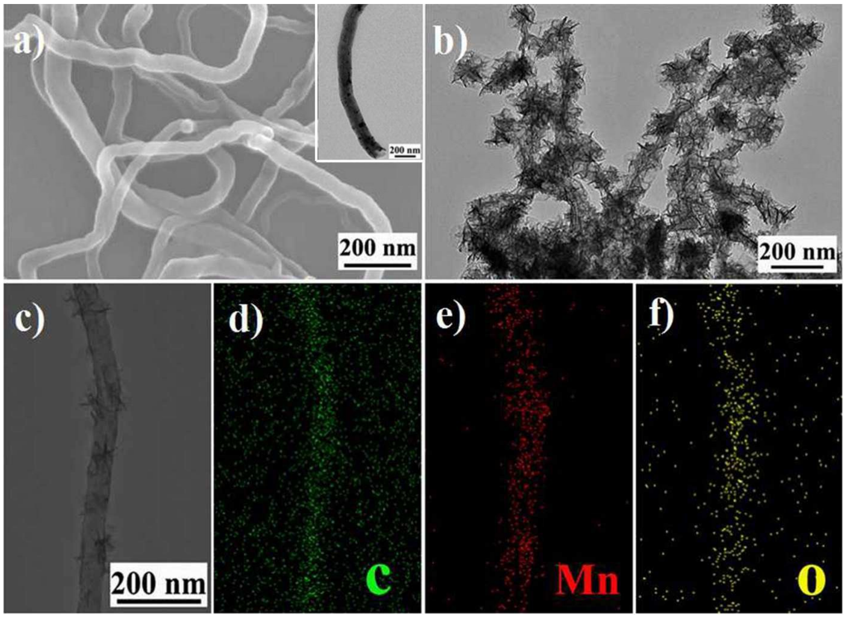

Fig. 6 (a) SEM and TEM images (inset) of MnO_2/CNTs hybrid nanostructures obtained after two hours of irradiation; (b) TEM image of MnO_2/CNTs hybrid nanostructures obtained after aging for 5 day in dark followed by the irradiation. (c-f) The elemental mapping images of the MnO_2/CNTs hybrid nanostructures.

example, the concentration of H^+ changed about four orders of magnitude when the pH values changed from 5 to 1 in Fig. 5, while the concentration of $KMnO_4$ solution only changed less than one order of magnitude from 0.01 M to 0.005 M in Fig. 4.

The optical sources were also changed from UV light to visible light to investigate their effect on the product morphology. It was found that hierarchical Bir-MnO_2 can also be successfully fabricated and exhibited no substantial morphological alteration (Fig. S3a and b). This result could be addressed on the basis of the UV-vis absorption spectra of $KMnO_4$ solutions. Fig. 2a indicates that $KMnO_4$ solution has two obvious absorption bands centered at 360 and 550 nm, which means that $KMnO_4$ could be excited and decomposed by both UV and visible light. This property makes the decomposition of $KMnO_4$ prone to achieve even under indoor light as shown in Fig. S3c and d. All the results proved that the shapes of the hierarchical nanostructure Bir-MnO_2 almost didn't change in different optical sources, indicating that the synthetic method was scalable and convenient.

In general, the Bir-MnO_2 nanosheets assembled 3D hierarchical nanostructures could be easily obtained without the addition of any surfactants or organic templates, while the size of the nanostructures could be easily controlled from dozens of nanometers to several micrometers. More interestingly, we found that the two steps involved in the formation of Bir-MnO_2 could be used as a strategy to decorate Bir-MnO_2 over different supports, such as carbon materials, to form composites with hierarchical nanostructures. Here, we demonstrated the practicability of deposition of Bir-MnO_2 on CNTs (Bir-MnO_2/CNTs hybrids), which have been emerged as a promising candidate in the applications of supercapacitors, Li-batteries and etc.[41, 42]

The preparation process was quite similar with that of Bir-MnO_2 as illustrated in Scheme 1b. The MnO_4^- was reduced to form small Bir-MnO_2 particles on the CNTs surface in the irradiation of UV light. The suspension then was placed in dark for 5 days to allow the further deposition of Bir-MnO_2. Before the experiments, we studied the interaction between $KMnO_4$ and CNTs, since the reaction between $KMnO_4$ and CNTs was possible according to the literature.[43, 44] CNTs were directly dispersed in the aqueous solution of $KMnO_4$ in dark at the temperature of 10 °C for a period of time. It was distinct that Bir-MnO_2 was difficult to decorate over CNTs in our experimental conditions.

Fig. 6a indicates that it is hard to find obvious hierarchical Bir-MnO_2 over CNTs after two hours of irradiation under UV light according to the SEM image. But the TEM image proved that small particles of Bir-MnO_2 were decorated on CNTs.

When the mixture was statically put in the dark for 5 days, MnO_2 nanosheets assembled hierarchical nanostructure uniformly decorated on the CNTs along the longitudinal axis of the nanotubes as shown in Fig. 6b. The elemental mapping images (Fig. 6c-f) further showed that both Mn and O elements were equably covered over the CNTs, confirming the uniformly decoration of Bir-MnO_2 over CNTs. XRD pattern (Fig. S4) also confirmed the formation of Bir-MnO_2.[45]

Conclusions

We have put forward a facile, green and low-cost strategy for controllable synthesis of Bir-MnO_2 nanosheets assembled “desert rose”-like 3D hierarchical nanostructure. Bir-MnO_2 was achieved by the direct decomposition of $KMnO_4$ with the assistance of photolysis and autocatalysis effect at room temperature. Two steps were involved in the formation of 3D hierarchical nanostructure. The first step was carried out in the irradiation of UV/Vis light to form curly and interlaced nanosheets. The formed Bir-MnO_2 nanosheets then act as seeds for further decomposition of the excess MnO_4^- in the dark, facilitating the formation of nanosheets assembled “desert rose”-like 3D hierarchical nanostructures. The size of the nanostructures could be conveniently adjusted by changing the pH value, the concentration of MnO_4^- and the light source. Encouragingly, Bir-MnO_2 nanosheets on CNTs have further been successfully fabricated utilizing the same strategy without the addition of any surfactants or organic templates. We believe this is a universal method for the fabrication of Bir-MnO_2 based composites and diverse functional nanomaterials.

Acknowledgements

This work was financially supported by the National Natural Science Foundation of China (21303099), the National Basic Research Program of China (973 Program, 2014CB660803) and the Major Program of Shanghai Science and Technology Committee (14DZ1207400).

Notes and references

1. L. Huang, X. Zhao, L. Zhang, L. Shi, J. Zhang and D. Zhang, *Nanoscale*, 2015, **7**, 2743-2749.
2. S. Cai, D. Zhang, L. Shi, J. Xu, L. Zhang, L. Huang, H. Li and J. Zhang, *Nanoscale*, 2014, **6**, 7346-7353.
3. Y. S. Ding, X. F. Shen, S. Gomez, H. Luo, M. Aindow and S. L. Suib, *Adv. Funct. Mater.*, 2006, **16**, 549-555.
4. Q. Zhang, W. Li, C. Moran, J. Zeng, J. Chen, L.-P. Wen and Y. Xia, *J. Am. Chem. Soc.*, 2010, **132**, 11372-11378.
5. L. Zhang, T. Xu, X. Zhao and Y. Zhu, *Appl. Catal. B: Environ.*, 2010, **98**, 138-146.
6. D. Chen, L. Cao, F. Huang, P. Imperia, Y.-B. Cheng and R. A. Caruso, *J. Am. Chem. Soc.*, 2010, **132**, 4438-4444.
7. R. Z. Ma, Y. Bando, L. Q. Zhang and T. Sasaki, *Adv. Mater.*, 2004, **16**, 918-922.
8. R. Renuka and S. Ramamurthy, *J. Power Sources*, 2000, **87**, 144-152.
9. W. Wei, X. Cui, W. Chen and D. G. Ivey, *Chem. Soc. Rev.*, 2011, **40**, 1697-1721.
10. L. Athouel, F. Moser, R. Dugas, O. Crosnier, D. Belanger and T. Brousse, *J. Phys. Chem. C*, 2008, **112**, 7270-7277.
11. J. Hou, Y. Li, M. Mao, L. Ren and X. Zhao, *ACS Appl. Mater. Inter.*, 2014, **6**, 14981-14987.
12. T. Rennert, A. Pohlmeier and T. Mansfeldt, *Environ. Sci. Technol.*, 2005, **39**, 821-825.
13. E. Eren, M. Guney, B. Eren and H. Gumus, *Appl. Catal. B: Environ.*, 2013, **132**, 370-378.
14. L. Al-Attar, A. Dyer and R. Harjula, *J. Mater. Chem.*, 2003, **13**, 2963-2968.
15. L. Dang, C. Wei, H. Ma, Q. Lu and F. Gao, *Nanoscale*, 2015, **7**, 8101-8109.
16. L. Wang and H. Cheng, *Environ. Sci. Technol.*, 2015, **49**, 3473-3481.
17. K. W. Nam, S. Kim, S. Lee, M. Salama, I. Shterenberg, Y. Gofer, J.-S. Kim, E. Yang, C. S. Park, J.-S. Kim, S.-S. Lee, W.-S. Chang, S.-G. Doo, Y. N. Jo, Y. Jung, D. Aurbach and J. W. Choi, *Nano Lett.* 2015, **15**, 4071-4079.
18. M. Huang, Y. Zhang, F. Li, L. Zhang, R. S. Ruoff, Z. Wen and Q. Liu, *Sci. Rep.*, 2014, **4**: 3878.
19. Y. Sun, L. Wang, Y. Liu and Y. Ren, *Small*, 2015, **11**, 300-305.
20. B. Ming, J. Li, F. Kang, G. Pang, Y. Zhang, L. Chen, J. Xu and X. Wang, *J. Power Sources*, 2012, **198**, 428-431.
21. H. T. Zhu, J. Luo, H. X. Yang, J. K. Liang, G. H. Rao, J. B. Li and Z. M. Du, *J. Phys. Chem. C*, 2008, **112**, 17089-17094.
22. H. Jiang, C. Li, T. Sun and J. Ma, *Nanoscale*, 2012, **4**, 807-812.
23. S.-B. Ma, K.-Y. Ahn, E.-S. Lee, K.-H. Oh and K.-B. Kim, *Carbon*, 2007, **45**, 375-382.
24. H. W. Chang, Y. R. Lu, J. L. Chen, C. L. Chen, J. F. Lee, J. M. Chen, Y. C. Tsai, C. M. Chang, P. H. Yeh, W. C. Chou, Y. H. Liou and C. L. Dong, *Nanoscale*, 2015, **7**, 1725-1735.
25. J. Yan, Z. Fan, T. Wei, W. Qian, M. Zhang and F. Wei, *Carbon*, 2010, **48**, 3825-3833.
26. L. Peng, X. Peng, B. Liu, C. Wu, Y. Xie and G. Yu, *Nano Lett.*2013, **13**, 2151-2157.
27. H. Jiang, C. Li, T. Sun and J. Ma, *Chem. Commun.*, 2012, **48**, 2606-2608.
28. J. Liu, J. Jiang, C. Cheng, H. Li, J. Zhang, H. Gong and H. J. Fan, *Adv. Mater*, 2011, **23**, 2076-2081.
29. C. X. Guo, M. Wang, T. Chen, X. W. Lou and C. M. Li, *Adv. Energy Mater.*, 2011, **1**, 736-741.
30. A. H. Webster and J. Halpern, *Trans. Faraday Soc.*, 1957, **53**, 51-60.
31. D. Portehault, S. Cassaignon, N. Nassif, E. Baudrin and J. P. Jolivet, *Angew. Chem. Int. Ed. Engl,* 2008, **47**, 6441-6444.
32. W. Xiao, D. Wang and X. W. Lou, *J. Phys. Chem. C*, 2010, **114**, 1694-1700.
33. W. Xiao, J. S. Chen, Q. Lu and X. W. Lou, *J. Phys. Chem. C*, 2010, **114**, 12048-12051.
34. K. Kai, Y. Yoshida, H. Kageyama, G. Saito, T. Ishigaki, Y. Furukawa and J. Kawamata, *J. Am. Chem. Soc.*, 2008, **130**, 15938-15943.
35. Y. Omomo, T. Sasaki, L. Wang, and M. Watanabe, *J. Am. Chem. Soc.*, 2003, **125**, 3568-3575.
36. Y. Oaki and H. Imai, *Angew. Chem. Int. Ed. Engl,* 2007, **46**, 4951-4955.
37. J. Zhu, Q. Li, W. Bi, L. Bai, X. Zhang, J. Zhou and Y. Xie, *J. Mater. Chem. A*, 2013, **1**, 8154-8159.
38. M. L. Chacón-Patiño, C. Blanco-Tirado, J. P. Hinestroza and M. Y. Combariza, *Green Chem.*, 2013, **15**, 2920-2928
39. S. L. Holt and C. J. Ballhausen, *Theoret. chim.* Acta, 1967, **7**,313-320.
40. F. Polzer, D. A. Kunz, J. Breu and M. Ballauff, *Chem. Mater.*, 2010, **22**, 2916-2922.
41. C. Jin, T. C. Nagaiah, W. Xia, B. Spliethoff, S. Wang, M. Bron, W. Schuhmann and M. Muhler, *Nanoscale*, 2010, **2**, 981-987.

42. J. Yan, Z. Fan, T. Wei, J. Cheng, B. Shao, K. Wang, L. Song and M. Zhang, *J. Power Sources*, 2009, **194**, 1202-1207.
43. X. Jin, W. Zhou, S. Zhang and G. Z. Chen, *Small*, 2007, **3**, 1513-1517.
44. M. Liu, W. W. Tjiu, J. Pan, C. Zhang, W. Gao and T. Liu, *Nanoscale*, 2014, **6**, 4233-4242.
45. H. Xia, M. Lai and L. Lu, *J. Mater. Chem.*, 2010, **20**, 6896-6902.

Graphical abstract

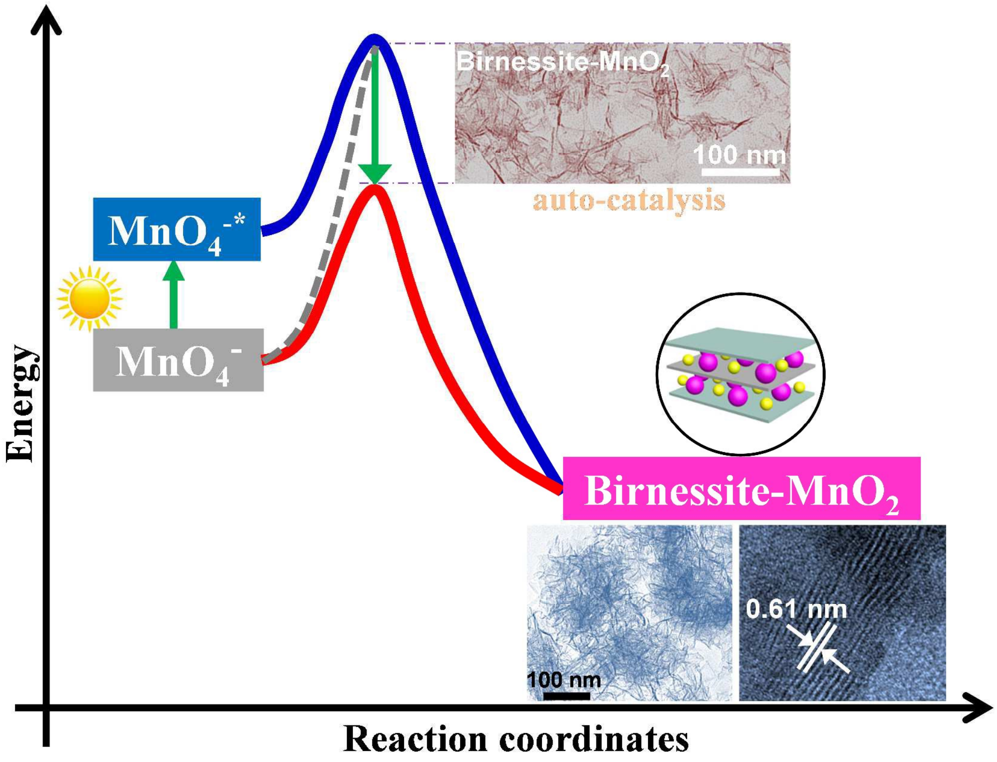

Layered birnessite-type MnO_2 nanosheets assembled hierarchical nanostructures were successfully fabrication by the direct decomposition of $KMnO_4$ with the assistance of photolysis and auto-catalysis effect.